18. Vanyúr, R., Biczók, L., and Miskolczy, Z., Micelle formation of 1-alkyl-3-methylimidazolium bromide ionic liquids in aqueous solution, *Colloids Surfaces A: Physicochem. Eng. Aspects* **299**, 256–261 (2007).
19. Anacker, E. W. and Ghose, H. M., Counterions and micelle size. II. Light scattering by solutions of cetylpyridinium salts, *J. Am. Chem. Soc.* **90**, 3161–3166 (1968).
20. Zana, R., *Surfactant Solutions: New Methods of Investigation*, Marcel Dekker, New York, 1986.
21. (a) Pádua, A. A. H. and Canongia Lopes, J. N., Nanostructural organization in ionic liquids, *J. Phys. Chem. B* **110**, 3330–3335 (2006). (b) Canongia Lopes, J. N., Costa Gomes, M. F., and Pádua, A. A. H., Nonpolar, polar, and associating solutes in ionic liquids, *J. Phys. Chem. B* **110**, 16816–16818 (2006).

4 Mass Spectrometric Studies on Ionic Liquid Aggregates

R. LOPES DA SILVA
Departamento de Química, Universidade de Aveiro, Aveiro, Portugal
I. M. MARRUCHO and J. A. P. COUTINHO
CICECO, Departamento de Química, Universidade de Aveiro, Aveiro, Portugal
ANA M. FERNANDES
QOPNA, Departamento de Química, Universidade de Aveiro, Aveiro, Portugal

Abstract

The association of ionic liquids to form aggregates was studied in detail by electrospray ionisation mass spectrometry (ESI-MS) and tandem mass spectrometry (ESI-MS-MS). The ESI-MS results show the formation of aggregates $[C_{n+1}(BF_4)_n]^+$, where C = $[C_{4-10}mim]^+$, $[C_2OHmim]^+$, and $[C_4dmim]^+$ with $n = 1$ up to 13 for all the ionic liquids investigated. The differences observed between the numbers of neutral molecules that will form the most stable aggregate ion were correlated with structural differences in the cations. The ESI-MS-MS experiments performed for each mass–selected aggregate at different collision energies (breakdown graphs) showed that their dissociation, in the gas phase, may not necessarily occur always by sequential loss of $n(CBF_4)$ units, but also by intact $(CBF_4)_n$ neutrals. The relative order of hydrogen bond strengths between cation and anion, in each ion pair of ionic liquids studied, was established using Cooks's kinetic method. The results indicate that the order of hydrogen bond strength to $[BF_4]^-$ is $[C_4dmim]^+ < [C_{10}mim]^+ < [C_8mim]^+ < [C_4mim]^+ < [C_2OHmim]^+$, and to $[PF_6]^-$ the order is $[C_4dmim]^+ < [C_8mim]^+ < [C_6mim]^+ < [C_4mim]^+$.

Molten Salts and Ionic Liquids: Never the Twain? Edited by Marcelle Gaune-Escard and Kenneth R. Seddon

4.1 INTRODUCTION

Ionic liquids have been the subject of an increasing number of publications due to their unique physicochemical properties: negligible vapour pressure, relatively low viscosity, high thermal and chemical stability, and distinct solubility in both polar and nonpolar solvents inter alia [1]. The wide range of applications of ionic liquids, as well as the possibility of their use as "green" alternatives to volatile organic solvents, justifies the interest of researchers on these compounds [2]. The knowledge of their structural organization in the liquid phase is of fundamental importance in the understanding of their properties [3]. On the basis of spectroscopic analysis [4–8] and ab initio calculations [9, 10], particularly on imidazolium-based ionic liquids, they have been described as polymeric supramolecules formed through hydrogen bonds of the imidazolium cation with the anion [11].

Electrospray ionisation mass spectrometry (ESI-MS) is a major technique for the analysis of positive and negative ions present in solution. A high voltage is applied to a metallic capillary through which the solution is flowing. If the counterelectrode is large and planar, the strength of the electric field at the capillary tip is typically about 10^6–$10^7\,V\,m^{-1}$. In the positive ion mode, anions migrate in the direction of the capillary, whereas cations migrate in the direction of the counterelectrode. At sufficiently high electric field strengths, a dynamic cone of liquid (referred to as a "Taylor cone") will form at the tip of the capillary. When the surface tension of the liquid does not compensate for the high charge density, a stream of droplets will emerge from the tip of the jet. As the solvent evaporates from the droplets with the assistance of warm nitrogen gas, the size of the droplets decreases until the electrostatic repulsion between the ions becomes equal to the surface tension and droplet fission occurs. Successive fissions will ultimately lead to the formation of gas phase ions that can be analysed within the mass spectrometer. A unique feature of this technique is the direct transfer to the gas phase of loosely bonded clusters of ions present in solution or formed in the droplets during the electrospray process [12, 13].

TABLE 4.1 Ionic Liquids Used in the Study

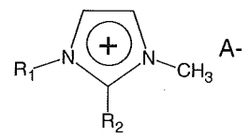

Ionic Liquid	R_1	R_2	A
$[C_4mim][BF_4]$	C_4H_9	H	BF_4
$[C_4mim][PF_6]$	C_4H_9	H	PF_6
$[C_6mim][PF_6]$	C_6H_{13}	H	PF_6
$[C_8mim][BF_4]$	C_8H_{17}	H	BF_4
$[C_8mim][PF_6]$	C_8H_{17}	H	PF_6
$[C_{10}mim][BF_4]$	$C_{10}H_{21}$	H	BF_4
$[C_4dmim][BF_4]$	C_4H_9	CH_3	BF_4
$[C_2OHmim][BF_4]$	C_2H_4OH	H	BF_4

The aim of the present work is to use electrospray ionisation mass spectrometry and tandem mass spectrometry to investigate the influence of structural features of the cations on the formation of imidazolium-based ionic liquid aggregates, their gas-phase dissociation, and the relative order of hydrogen-bond strengths between cation and anion in each ion pair of ionic liquids studied (Table 4.1).

4.2 EXPERIMENTAL

The ionic liquids shown in Table 4.1 were used as ethanenitrile solutions (1.5×10^{-4} M). Electrospray ionisation mass (ESI-MS) and tandem mass spectra (ESI-MS-MS) were acquired with a Micromass Q-ToF 2 operating in the positive ion mode. Source and desolvation temperatures were 80 °C and 100 °C, respectively. The capillary voltage was 2600 V and cone voltage was 25 V. ESI-MS-MS spectra were acquired by selecting the precursor ion with the quadrupole, performing collisions with argon at energies of 2–30 eV in the hexapole, followed by mass analysis of product ions by the ToF analyser. N_2 was used as the nebulisation gas. The ionic liquid solutions were introduced at a $10\,\mu L \cdot min^{-1}$ flow. The breakdown graphs were obtained by acquiring the ESI-MS-MS spectra of each ion investigated at increasing collision energies and plotting the relative abundance of precursor and fragment ions as a function of collision energy. The relative order of hydrogen-bond strength between cation and anion in each ion pair studied was obtained by acquiring the ESI-MS-MS spectra, at 10 eV collision energy, of the cluster ions $[C_1 \cdots A \cdots C_2]^+$, and measuring the relative abundances of the two fragment ions observed.

4.3 RESULTS AND DISCUSSION

4.3.1 ESI Mass Spectra

The electrospray ionisation mass spectrum in the positive ion mode of the ionic liquids $[C_{4-10}mim][BF_4]$, $[C_4dmim][BF_4]$, and $[C_2OHmim]BF_4]$ showed peaks corresponding to the formation of aggregates $[C_{n+1}(BF_4)_n]^+$ with $n = 1$ up to 13, in agreement with previously published results [11, 14]. The formation of an aggregate whose intensity does not follow the normal decreasing pattern has been observed for all the ionic liquids investigated. The spectrum of $[C_{10}mim][BF_4]$, shown in Figure 4.1, exemplifies this behaviour with the out-of-range abundance of ion $[(C_{10}mim)_5(BF_4)_4]^+$ (m/z 1464), which corresponds to $n = 4$ in the general formula $[C_{n+1}(BF_4)_n]^+$. An increased gas phase stability of this particular ion as compared with its neighbours explains its greater relative abundance in the mass spectrum. Whereas the size of the *N*–alkyl side chain does not seem to have any effect on the composition of the most stable aggregate, which was $[(C_5A_4)]^+$ when $C = [C_{4-10}mim]^+$, for the ionic liquids with a methyl group at position C_2 of the imidazolium ring, or with a functionalised side chain with OH, the value of n decreased to three.

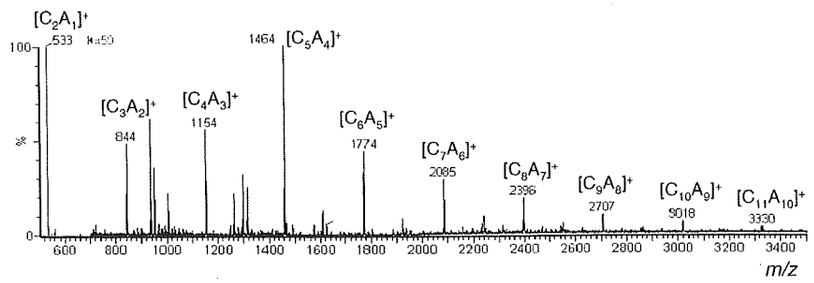

FIGURE 4.1 Electrospray ionisation mass spectrum of $[C_{10}mim][BF_4]$.

4.3.2 ESI-MS-MS Spectra and Breakdown Graphs

The ESI-MS-MS spectra of all mass-selected aggregates $[C_{n+1}(BF_4)_n]^+$ activated by collision with argon show peaks at mass intervals corresponding to a neutral "molecule" of ionic liquid. This observation can be interpreted as a sequential loss, by the precursor ion, of $n(CBF_4)$ units, or as loss of individual $(CBF_4)_n$ units. In order to obtain a better understanding of the fragmentation dynamics of ionic liquid aggregates, the dependence of the ESI-MS-MS spectra on collision energy was investigated. Treatment of data by plotting the relative abundances of precursor and fragment ions as a function of collision energy (eV) affords the breakdown graphs [15] exemplified in Figures 4.2–4.4 for $[(C_4mim)_4(BF_4)_3]^+$, $[(C_4mim)_5(BF_4)_4]^+$, and $[(C_4mim)_6(BF_4)_5]^+$, respectively.

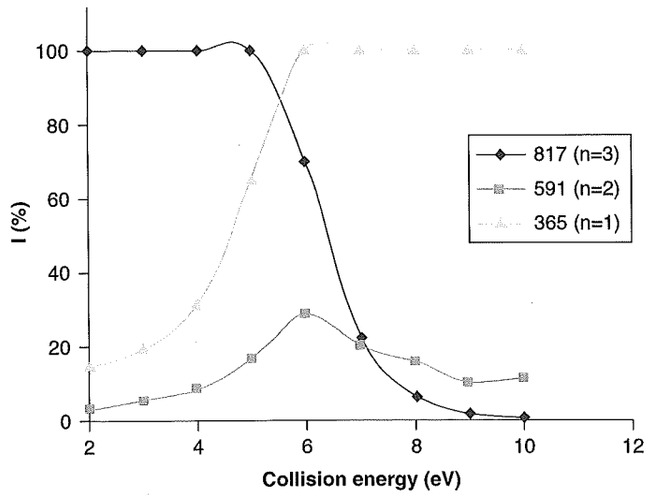

FIGURE 4.2 Breakdown graphs for $[(C_4mim)_4(BF_4)_3]^+$.

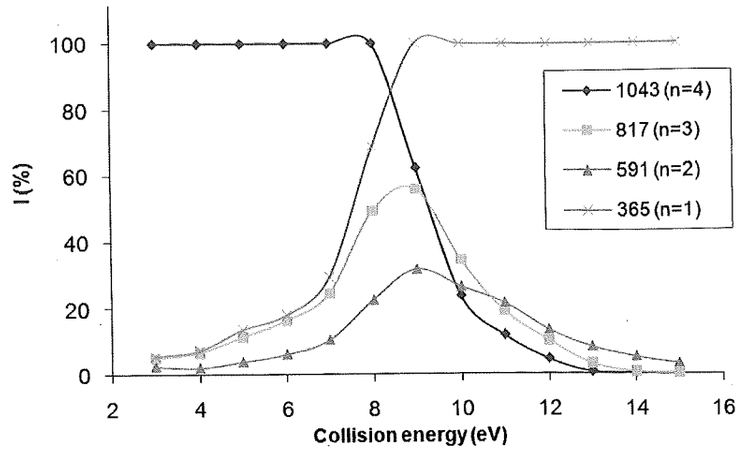

FIGURE 4.3 Breakdown graphs for $[(C_4mim)_5(BF_4)_4]^+$.

The breakdown pattern of ion $[(C_4mim)_4(BF_4)_3]^+$ (*m/z* 817; Fig. 4.2) shows a decay of its relative abundance and, at relatively low collision energies, coformation of ions *m/z* 591 and *m/z* 365, by loss of one or two neutral molecules, respectively, indicating that a direct loss of $([C_4mim][BF_4])_2$ from the precursor ion can occur. As the collision energy increases, the relative abundances of *m/z* 817 and 591 decrease, and ions *m/z* 365 become more abundant.

Figure 4.3 provides further evidence for the loss of neutral $([C_4mim][BF_4])_n$ with $n = 1$–3 from $[(C_4mim)_5(BF_4)_4]^+$ (*m/z* 1043). Since the maximum abundance for ions *m/z* 817 and *m/z* 591 occurs at roughly the same collision energy, it can be

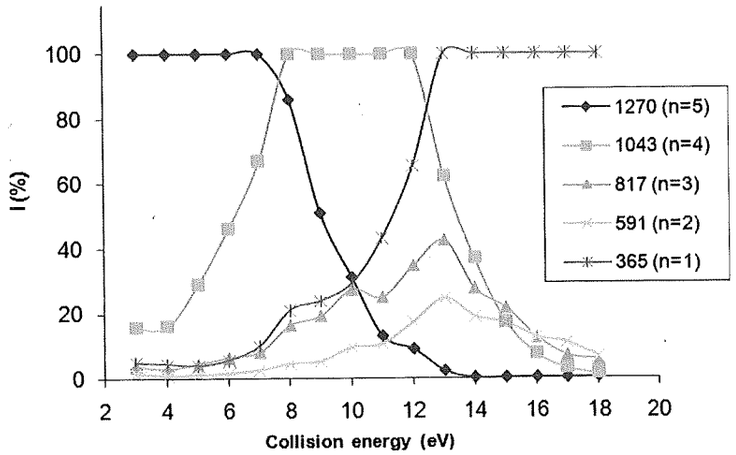

FIGURE 4.4 Breakdown graphs for $[(C_4mim)_6(BF_4)_5]^+$.

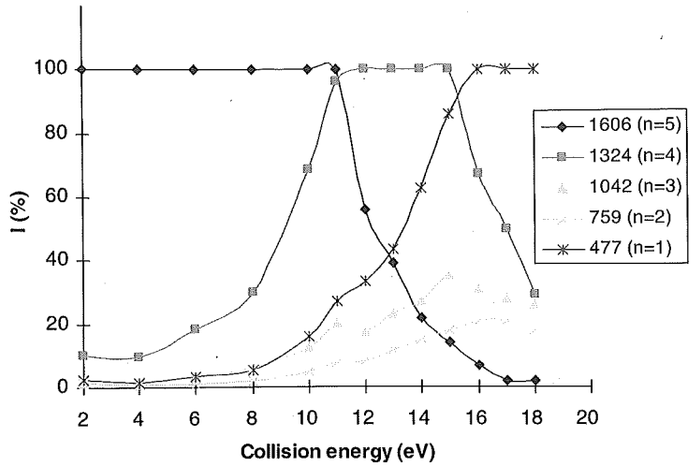

FIGURE 4.5 Breakdown graphs for $[(C_8mim)_6(BF_4)_5]^+$.

assumed that both will decompose, at higher collision energies, to $[(C_4mim)_2(BF_4)]^+$ (*m/z* 365) by loss of two or one neutral molecules, respectively, in agreement with the observations of Figure 4.2.

Interpretation of Figure 4.4 indicates a relative abundant formation of ion $[(C_4mim)_5(BF_4)_4]^+$ (*m/z* 1043), together with initial coformation of the low abundant ions *m/z* 817, 591, and 365 consistent with losses of $([C_4mim][BF_4])_n$ neutrals with $n = 1$ to 4. The predominance of ion *m/z* 1043 with 100% of relative abundance between 8 and 12 eV collision energy is noteworthy and consistent with the ESI

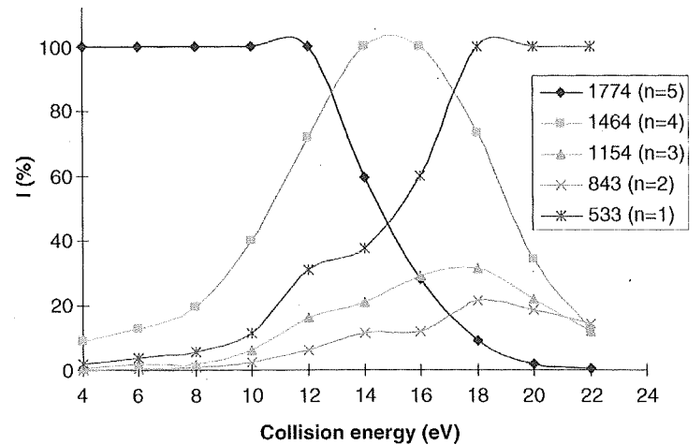

FIGURE 4.6 Breakdown graphs for $[(C_{10}mim)_6(BF_4)_5]^+$.

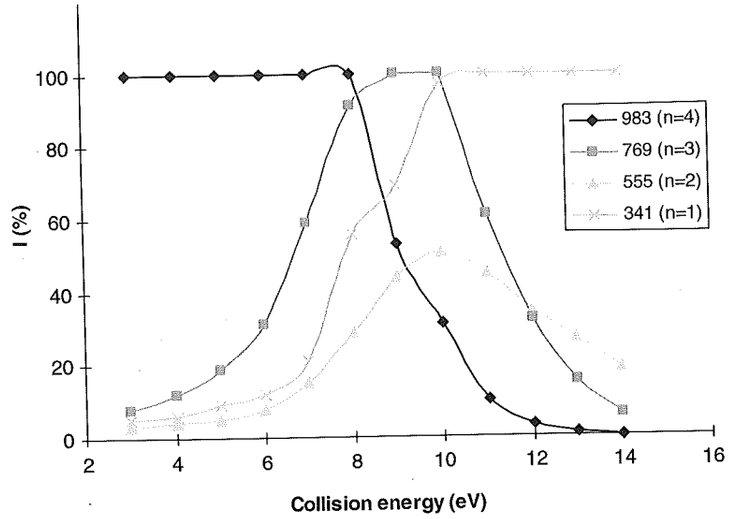

FIGURE 4.7 Breakdown graphs for $[(C_2OHmim)_5(BF_4)_4]^+$.

spectrum of $[C_4mim][BF_4]$, where that ion was identified as the most stable aggregate. At higher collision energies, the decay and formation of the ions shown in Figure 4.4 are almost a replica of those shown in Figure 4.3.

Since the most favoured assemblies of the ionic liquids $[C_8mim][BF_4]$ and $[C_{10}mim][BF_4]$ also correspond to $n = 4$ in the general formula $[C_{n+1}A_n]^+$, the breakdown graphs of ions $[(C_8mim)_6(BF_4)_5]^+$ and $[(C_{10}mim)_6(BF_4)_5]^+$ for these two ionic liquids are shown on Figures 4.5 and 4.6 for comparison with Figure 4.4. The pattern of decay and formation of the ions for these three ionic liquids are very similar: coformation of low abundant ions corresponding to losses of $([C_4mim][BF_4])_n$ neutrals with $n = 2$–4, and a predominant and more stable ion corresponding to $n = 4$.

For the two ionic liquids where $n = 3$, the comparison that has to be done is between the breakdown graphs of ions $[(C_2OHmim)_5(BF_4)_4]^+$ and $[(C_4dmim)_5(BF_4)_4]^+$ (Figs. 4.7 and 4.8) and those of Figures 4.4–4.6. The conclusions drawn are identical to the ones mentioned in the previous paragraph, particularly in what concerns the behaviour of the ions corresponding to the most stable aggregates for the five ionic liquids studied.

The interpretation of the above breakdown graphs represents a strong indication that the collision-induced dissociation of ionic liquid aggregates can proceed via loss of $([C_4mim][BF_4])_n$ neutral molecules, where n can vary from 1 to 4, and not as a sequential decay via $n([C_4mim][BF_4])$ units.

4.3.3 Relative Hydrogen Bond Strengths by Cooks's Kinetic Method

The kinetic method of making thermochemical determinations proposed by Cooks [16–18] is based on the relative rates of competitive dissociations of a cluster

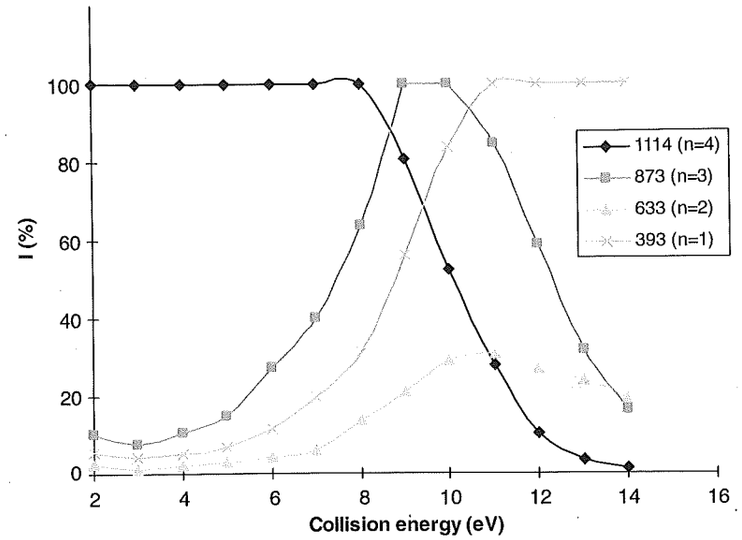

FIGURE 4.8 Breakdown graphs for $[(C_4dmim)_5(BF_4)_4]^+$.

ion comprised of the compound of interest and a reference compound. For example, the cluster ion $[B_1 \cdots H^+ \cdots B_2]$ dissociates as shown in Eq. (4.1):

$$B_1 \cdots H^+ \cdots B_2 \xrightarrow{k_1} B_1H^+ + B_2 \qquad B_1 \cdots H^+ \cdots B_2 \xrightarrow{k_2} B_2H^+ + B_1 \tag{4.1}$$

where k_1 and k_2 are the rate constants for the competitive dissociations of the cluster ion to yield $[B_1H]^+$ and $[B_2H]^+$, respectively. The major assumptions of the method are the following:

- Negligible differences in the entropy requirements for the competitive channels
- Negligible reverse activation energies
- Absence of isomeric forms of the activated cluster ion

When these conditions are satisfied, the rates of the dissociations are controlled by the relative activation energies of each reaction channel, the difference in which is equivalent to the differences in proton affinities, $\Delta(\Delta H)$, of the two bases B_1 and B_2. Experimentally, the method can be performed using any tandem mass spectrometer by mass selection of the cluster ion $[B_1 \cdots H^+ \cdots B_2]$ and analysis of its fragmentation products. If no secondary reactions occur, the relative abundances of the fragment ions $[B_1H]^+$ and $[B_2H]^+$ will be determined by the rate constants k_1 and

k_2, respectively. Hence the ratio of the fragment ion abundances will be related to $\Delta(\Delta H)$:

$$\ln\frac{k_1}{k_2} = \ln\left[\frac{B_1H^+}{B_2H^+}\right] \approx \frac{\Delta(\Delta H)}{RT_{\text{eff}}} \tag{4.2}$$

where T_{eff} is the effective temperature of the activated dimer. A plot of $\ln(k_1/k_2)$ versus $\Delta(\Delta H)$ for a set of reference compounds of known proton affinity will produce a straight line of slope $1/RT_{\text{eff}}$. From such a plot, the proton affinity of an unknown compound can be obtained by dissociation of the cluster ion formed by the unknown and a reference compound. A qualitative application of the method will produce a relative order of proton affinities (or other thermochemical quantities) in the following way: first the cluster ion $[B_1 \cdots H^+ \cdots B_2]$ produced in the ionisation source of the mass spectrometer will be selected in the first analyser, dissociated in a collision cell, and the fragmentation products analysed in the second mass analyser. If, for example, the proton affinity of B_1 is greater than the proton affinity of B_2, the loss of the neutral molecule B_2 will be favoured, and the relative abundance of ion $[B_1H]^+$ will be greater than that of ion $[B_2H]^+$. The analysis of several combinations of B_1 and B_2 will establish a relative order of proton affinities for the bases under study.

In the present study, the kinetic method was used to establish a relative order of hydrogen-bond strengths in the cation–anion ion pairs of imidazolium-based ionic liquids. Tetrafluoroborate, $[BF_4]^-$, and hexafluorophosphate, $[PF_6]^-$, were used as anions, $[A]^-$; and $[C_4mim]^+$, $[C_6mim]^+$, $[C_8mim]^+$, $[C_{10}mim]^+$, $[C_4dmim]^+$, and $[C_2OHmim]^+$ were used as cations, $[C]^+$. Equimolar mixtures of two ionic liquids in ethanenitrile were introduced into the electrospray ion source, the clusters $[C_1 \cdots A \cdots C_2]^+$ were selected with the quadrupole and dissociated by 10 eV collisions with argon, and the product ions were analysed with the ToF. Tables 4.2 and 4.3 present the results obtained for the binary mixtures of ionic liquids used to form the clusters. The ESI-MS-MS spectrum of the cluster $[C_4mim \cdots BF_4 \cdots C_8mim]^+$ (*m/z* 479; Fig. 4.9) shows that a stronger hydrogen bond of the ion pair $[C_4mim]^+ \cdots [BF_4]^-$ will favour the loss of the neutral molecule $[C_4mim][BF_4]$ from the cluster, which results in a greater abundance of ion $[C_8mim]^+$ (*m/z* 195) as compared with $[C_4mim]^+$ (*m/z* 139).

The analysis of the data in Tables 4.2 and 4.3 assumes, as explained earlier, that a stronger hydrogen bond of the ion pair will generate a less abundant cation in the ESI-MS-MS spectrum of the cluster. Thus the order of hydrogen-bond strength to $[BF_4]^-$ is

$$[C_4dmim]^+ < [C_{10}mim]^+ < [C_8mim]^+ < [C_4mim]^+ < [C_2OHmim]^+$$

and to $[PF_6]^-$ is

$$[C_4dmim]^+ < [C_8mim]^+ < [C_6mim]^+ < [C_4mim]^+$$

TABLE 4.2 Relative Abundances[a] of the Imidazolium Cations in the ESI-MS-MS Spectra of the Clusters $[C_1 \cdots BF_4 \cdots C_2]^+$

Cation	$[C_4mim]^+$	$[C_8mim]^+$
Relative abundance / %	31.3	100
Cation	$[C_4mim]^+$	$[C_{10}mim]^+$
Relative abundance / %	23.9	100
Cation	$[C_4mim]^+$	$[C_4dmim]^+$
Relative abundance / %	7.1	100
Cation	$[C_4mim]^+$	$[C_2OHmim]^+$
Relative abundance / %	64.7	14.9
Cation	$[C_8mim]^+$	$[C_{10}mim]^+$
Relative abundance / %	82.1	100
Cation	$[C_8mim]^+$	$[C_4dmim]^+$
Relative abundance / %	14.7	100
Cation	$[C_8mim]^+$	$[C_2OHmim]^+$
Relative abundance / %	100	4.4
Cation	$[C_{10}mim]^+$	$[C_4dmim]^+$
Relative abundance / %	17.4	100
Cation	$[C_{10}mim]^+$	$[C_2OHmim]^+$
Relative abundance / %	100	3.4
Cation	$[C_4dmim]^+$	$[C_2OHmim]^+$
Relative abundance / %	100	0.6

[a] Percentage % of the base peak.

These trends can be explained in terms of chain length increase on the N^1-alkyl group of the imidazolium, presence of a methyl group at C^2, and an OH-functionalised alkyl chain. A recent publication concerning the optimised structures of cation–anion ion pairs of 1,3-dialkylimidazolium-based ionic liquids at the B3LYP/6-31 + G level of

TABLE 4.3 Relative Abundances[a] of the Imidazolium Cations in the ESI-MS-MS Spectra of the Clusters $[C_1 \cdots PF_6 \cdots C_2]^+$

Cation	$[C_4mim]^+$	$[C_6mim]^+$
Relative abundance / %	44.2	100
Cation	$[C_4mim]^+$	$[C_8mim]^+$
Relative abundance / %	25.4	100
Cation	$[C_4mim]^+$	$[C_4dmim]^+$
Relative abundance / %	6.8	100
Cation	$[C_6mim]^+$	$[C_8mim]^+$
Relative abundance / %	47.3	64.4
Cation	$[C_6mim]^+$	$[C_4dmim]^+$
Relative abundance / %	16.5	100
Cation	$[C_8mim]^+$	$[C_4dmim]^+$
Relative abundance / %	22.1	100

[a] Percentage (%) of the base peak.

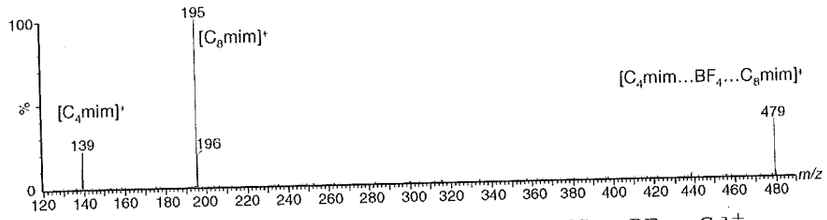

FIGURE 4.9 ESI-MS-MS spectrum of the cluster $[C_1 \cdots BF_4 \cdots C_2]^+$.

DFT theory [19] concluded that there were two stable hydrogen bonds, between the C^2–H of the imidazolium ring and one fluorine atom of the anion, and between a C–H of the side chain and another fluorine atom of the anion. Calculations of bond distances, bond angles, and interaction energies for the ion pairs $[C_{1-4}mim][BF_4]$ and $[C_{1-4}mim][PF_6]$ showed that with the increase in the size of the *N*-alkyl side chains, the distances of both H. . .F interactions increase, and the interaction energies between the cation and anion decrease. These conclusions are in complete agreement with the experimental results for the relative order of hydrogen-bond strength of cations to $[BF_4]^-$ (or $[PF_6]^-$) presented here. In $[C_4dmim][BF_4]$ or $[C_4dmim][PF_6]$, the C^2 position is blocked by a methyl group that not only decreases the hydrogen-bond donor ability [19, 20] of the cation but may represent a steric factor to the approach of either anion to the cation. Hence this gives the weakest hydrogen bond for these ion pairs. The strongest is, as expected, in $[C_2OHmim][BF_4]$, since a shorter chain length with a terminal OH group will favour the interaction between the cation and the two fluorine atoms.

4.4 CONCLUSION

Aggregates of imidazolium-based ionic liquids of the general formula $[C_{n+1}(BF_4)_n]^+$, where $C = [C_{4-10}mim]^+$, $[C_2OHmim]^+$, and $[C_4dmim]^+$ with $n = 1$ up to 13, were identified by electrospray ionisation mass spectrometry, which also shows the formation of assemblies with extra stability for $n = 4$ or 3 depending on the cation. The dependence of $[C_{4-6}(BF_4)_{3-5}]^+$ aggregates gas phase dissociation with collision energy gives a strong indication that they decompose via losses of intact $(CBF_4)_n$ neutrals where $n = 1$–4. The relative hydrogen-bond strengths between the imidazolium cation and the anion, postulated for the formation of polymeric structures in the liquid state, was established using Cooks's kinetic method. For the six imidazolium cations studied, the relative order of hydrogen bond strengths to $[BF_4]^-$ is $[C_4dmim]^+ < [C_{10}mim]^+ < [C_8mim]^+ < [C_4mim]^+ < [C_2OHmim]^+$ and to $[PF_6]^-$ it is $[C_4dmim]^+ < [C_8mim]^+ < [C_6mim]^+ < [C_4mim]^+$. The chain length increase on the N^1-alkyl group of the imidazolium, the presence of a methyl group at C^2, and an OH-functionalised alkyl chain explain these trends.

REFERENCES

1. Chiappe, C. and Pieraccini, D., Ionic liquids: solvent properties and organic reactivity, *J. Phys. Org. Chem.* **18**, 275–297 (2005).
2. Anderson, J. L., Armstrong, D. W., and Wei, G., Ionic liquids in analytical chemistry, *Anal. Chem.* **78**, 2892–2902 (2006).
3. Hardacre, C., McMath, S. E. J., Nieuwenhuyzen, M., Bowron, D. T., and Soper, A. K., Liquid structure of 1,3-dimetyhylimidazolium salts, *J. Phys. Condens. Matter* **15**, S159–S166 (2003).
4. Lee, K. M., Chang, H., Jiang, J., Lu, L. Hsiao, C., Lee, Y., Lin, S. H., and Lin, I. J. B., Probing C–H···X hydrogen bonds in amide-functionalized imidazolium salts under high pressure, *J. Chem. Phys.* **120**, 8645–8650 (2004).
5. Dupont, J., Suarez, P. A. Z., De Sousa, R. F., Burrow, R. A., and Kintzinger, J., C–H-p interactions in 1-*n*-butyl-3-methylimidazolium tetraphenylborate molten salt: solid and solution structures, *Chem. Eur. J.* **6**, 2377–2381 (2000).
6. Hardacre, C., Holbrey, J. D., McMath, S. E. J., Bowron, D. T., and Soper, A. K., Structure of molten 1,3-dimethylimidazolium chloride using neutron diffraction, *J. Chem. Phys.* **118**, 273–278 (2003).
7. Consorti, C. S., Suarez, P. A. Z., De Souza, R. F., Burrow, R. A., Farrar, D. H., Lough, A. J, Loh, W., Silva, L. H. M., and Dupont, J., Identification of 1,3-dialkylimidazolium salt supramolecular aggregates in solution, *J. Phys. Chem. B.* **109**, 4341–4349 (2005).
8. Dorbritz, S., Ruth, W., and Krafl, U., Investigation on aggregate formation of ionic liquids, *Adv. Synth. Catal.* **347**, 1273–1279 (2005).
9. Hunt, P. A., Kirchner, B., and Welton, T., Characterising the electronic structure of ionic liquids: an examination of the 1-butyl-3-methylimidazolium chloride ion pair, *Chem Eur. J.* **12**, 6762–6775 (2006).
10. Del Pópolo, M. G., Lynden-Bell, R. M., and Kohanoff, J., Ab initio molecular dynamics simulation of a room temperature ionic liquid, *J. Phys. Chem.* **109**, 5895–5902 (2005).
11. Abdul-Sada, A. K., Elaiwi, A. E., Greenway, A. M., and Seddon, K. R., Evidence for the clustering of substituted imidazolium salts via hydrogen bonding under the conditions of fast atom bombardment mass spectrometry, *Eur. Mass Spectrom.* **3**, 245–247 (1997); Dupont, J., On the solid, liquid and solution structural organization of imidazolium ionic liquids, *J. Braz. Chem. Soc.* **15**, 341–350 (2004).
12. Cole, R. R. B. (Ed.), *Electrospray Ionization Mass Spectrometry: Fundamentals, Instrumentation and Applications*, John Wiley & Sons, Hoboken, NJ, 1997.
13. Meng, C. K. and Fenn, J. B., Formation of charged clusters during electrospray ionization of organic solute species, *Org. Mass Spectrom.* **26**, 542–549 (1991).
14. Gozzo, F. C., Santos, L. S., Augusti, R., Consorti, C. S, Dupont, J., and Eberlin, M. N., Gaseous supramolecules of imidazolium based ionic liquids: "magic" numbers and intrinsic strengths of hydrogen bonds, *Chem. Eur. J.* **10**, 6187–6193 (2004).
15. Herzschuh, R. and Drewello, T., The fragmentation dynamics of small $Cs(CsI)_n^+$ cluster ions under low-energy multiple collision conditions, *Int. J. Mass Spectrom.* **233**, 355–359 (2004).
16. McLuckey, S. A., Cameron, D., and Cooks, R. G., Proton affinities from dissociations of proton-bound dimmers, *J. Am. Chem. Soc.* **103**, 1313–1317 (1981).

17. Cooks, R. G. and Wong, P. S. H., Kinetic method of making thermochemical determinations: advances and applications, *Acc. Chem. Res.* **31**, 379–386 (1998).
18. Cooks, R. G., Koskinen, J. T., and Thomas, P. D., The kinetic method of making thermochemical determinations, *J. Mass Spectrom.* **34**, 85–92 (1990).
19. Dong, K., Zhang, S., Wang, D., and Yao, X., Hydrogen bonds in imidazolium ionic liquids, *J. Phys. Chem. A* **110**, 9775–9782 (2006).
20. Crowhurst, L., Mawdsley, P. R., Perez-Arlandis, J. M., Salter, P. A., and Welton, T., Solvent–solute interactions in ionic liquids, *Phys. Chem. Chem. Phys.* **5**, 2790–2794 (2003).